defined concentric rings of Q degradation centered at two different locations in the nanotube are observed, corresponding to two distinct quantum dots. No electrical signal needs to be applied to the tube in this measurement, making it possible to measure tubes that are not electrically connected to external wires (*27*). Measurements on a number of samples show that multiple-dot behavior is quite common, with dot sizes ranging from <0.2 μm to >1.5 μm (with an average of 0.5 μm) in the six devices studied.

Finally, we turn our attention to the electrostatic information about the device that can be obtained by monitoring the charge state of the dot while varying both the tip position and the tip voltage. We restrict our discussion to *e*-SGM, but our comments are valid for the *e*-EFM techniques as well. A sequence of *e*-SGM images at different values of V_{tip} is shown in Fig. 3, concentrating on the dot on the right side of Fig. 2A. At large negative V_{tip} (Fig. 3A), a series of rings is seen that corresponds to the removal of electrons from the dot as the tip approaches the dot, whereas at large positive V_{tip} (Fig. 3H), concentric rings corresponding to the addition of electrons are seen. The features evolve continuously with V_{tip} between these limits but become complex near $V_{tip} \sim 100$ mV. For example, in Fig. 3I we show the number of electrons induced on the dot as a function of tip position at $V_{tip} = 150$ mV. We see that the tip can either add or subtract electrons from the dot, depending on its position.

A full explanation of the behavior shown in Fig. 3 is beyond the scope of this report, but its origin can be understood qualitatively by considering the effects of the electrostatic environment of the quantum dot. In addition to the charge induced on the dot by the AFM tip, charge is also induced by electric fields from the contacts, the backgate, and any fixed charges nearby on the sample. As the conducting tip moves over the sample, it screens these fields, changing the charge induced on the dot by the environment. It is the screening of these fields that gives rise to the complex spatial variation in the charge states of the dot. The effects of screening are most pronounced when the electrostatic potential difference between the tip and the dot is close to zero (here, when $V_{tip} \sim$ 100 to 200 mV). In this situation, the tip has little direct effect on the dot; instead, its main effect is to screen the dot from its electrostatic environment. This result emphasizes an important lesson: Although scanned probe techniques have the exquisite sensitivity needed to image single electrons in nanostructures, they almost invariably alter the properties of the system they are measuring (*4*, *6*, *11*).

References and Notes

1. H. Grabert, M. H. Devoret, Eds., *Single Charge Tunneling* (Plenum, New York, 1992).
2. L. P. Kouwenhoven *et al.*, in *Mesoscopic Electron Transport*, L. L. Sohn, L. P. Kouwenhoven, G. Schön, Eds. (Kluwer, Dordrecht, Netherlands, 1997).
3. S. H. Tessmer, P. I. Glicofridis, R. C. Ashoori, L. S. Levitov, M. R. Melloch, *Nature* **392**, 51 (1998).
4. G. Finkelstein, P. I. Glicofridis, R. C. Ashoori, M. Shayegan, *Science* **289**, 90 (2000).
5. M. J. Yoo *et al.*, *Science* **276**, 579 (1997).
6. N. B. Zhitenev *et al.*, *Nature* **404**, 473 (2000).
7. C. Schönenberger, S. F. Alvarado, *Phys. Rev. Lett.* **65**, 3262 (1990).
8. A. Bachtold *et al.*, *Phys. Rev. Lett.* **84**, 6082 (2000).
9. R. Crook, C. G. Smith, M. Y. Simmons, D. A. Ritchie, *J. Phys. C* **12**, L167 (2000).
10. M. A. Topinka *et al.*, *Science* **289**, 2323 (2000).
11. M. T. Woodside *et al.*, *Phys. Rev. B* **64**, 1310 (2001).
12. S. J. Tans, C. Dekker, *Nature* **404**, 834 (2000).
13. M. Bockrath, W. J. Liang, D. Bozovic *et al.*, *Science* **291**, 283 (2001).
14. K. L. McCormick *et al.*, *Phys. Rev. B* **59**, 4654 (1999).
15. J. Kong, H. T. Soh, A. M. Cassell, C. F. Quate, H. J. Dai, *Nature* **395**, 878 (1998).
16. M. Bockrath *et al.*, *Science* **275**, 1922 (1997).
17. S. J. Tans *et al.*, *Nature* **386**, 474 (1997).

18. When the tip is very close to the surface, it occasionally causes surface charges to move, producing irreversible changes in the device properties. All measurements are therefore made at heights above 100 nm.
19. We observe no obvious topographic features in the tube between the dots, where the tunnel barrier is located.
20. A typical cantilever used in these measurements has a resonant frequency $\omega_0 \sim 2 \times 10^5$ s^{-1}, a spring constant $k \sim 3$N/m, and a quality factor $Q \sim 30{,}000$.
21. D. Sarid, *Scanning Force Microscopy* (Oxford Univ. Press, Oxford, 1994).
22. C'_{td} is determined from *e*-SGM measurements of C_{td} as a function of the tip height.
23. The sensitivity expressed as a function of charge for the conditions here is ~0.03*e*, comparable to that of other scanned probe techniques that have been used to sense single charges (*3*, *5*). *e*-EFM measurements do perturb the charge on the dot, because of the dc tip-dot bias ΔV. The smallest ΔV practical for measurements is ~100 mV, which adds about four electrons to the dot. This is the same size of perturbation that results from the screening of the electrostatic environment of the dot, so *e*-EFM is not much more perturbative than any conducting scanned probe tip would be.
24. The derivative df/dq can be obtained from the conductance G, because each conductance peak has the form $G(q) = G_{max} \cdot (edf/dq)$ (*1*). For transport through a single energy level, f is just the Fermi distribution function.
25. The voltage is applied to the electrodes, and not the tip, for experimental convenience.
26. For a highly conducting dot like the one shown in Fig. 1A ($\mathcal{T} \sim 0.1 - 0.01$), Eq. 4 predicts an immeasurably small Q degradation ($\delta Q/Q \sim 10^{-5}$ to 10^{-6}). In fact, however, we observe a small but measurable signal ($\delta Q/Q \sim 0.02$). This indicates that other dissipative processes are also present in the experiment. For example, nonlinear electrostatic interactions between the tip and dot may produce coupling to other vibrational modes of the cantilever.
27. This is the case if the dot is electrically connected to somewhere the electron can go, such as another quantum dot or a single contact.

28. We thank J. Park, P. Kim, C. Vale, and M. Fuhrer for help with device preparation. Supported by the U.S. Department of Energy, Basic Energy Sciences, Materials Science Division, sp^2 Materials Initiative; and NSF.

16 January 2002; accepted 4 April 2002

Creation and Manipulation of Three-Dimensional Optically Trapped Structures

M. P. MacDonald,[1] L. Paterson,[1] K. Volke-Sepulveda,[2] J. Arlt,[3] W. Sibbett,[1] K. Dholakia[1]*

An interferometric pattern between two annular laser beams is used to construct three-dimensional (3D) trapped structures within an optical tweezers setup. In addition to being fully translatable in three dimensions, the trapped structure can be rotated controllably and continuously by introducing a frequency difference between the two laser beams. These interference patterns could play an important role in the creation of extended 3D crystalline structures.

At a microscopic level, transparent objects can be trapped and manipulated using the forces exerted by a tightly focused laser beam. This technique, known as "optical tweezers" (*1*, *2*), has enabled major advances in numerous areas of science, including force detection measurements on biological samples, such as the determination of the elastic response of DNA (*3*). Recent work has also demonstrated the use of optical tweezers for developing optical micromachines and micro-components (*4*–*8*). In parallel with this, the extension of optical tweezers to multiple beam sites to create two-dimensional particle arrays (*9*, *10*) has been investigated. We take this technique a step further by creating vertical arrays of particles (stacking) in multiple trapping sites, forming the basis for creating 3D trapped structures.

Stacking of a small number of particles in standing-wave geometries (*11*) and Bessel light beams (*12*) has been observed experimentally, whereas Gauthier and Ashman theoretically predicted stacking in a Gaussian beam (*13*). Experimentally, we have observed controlled stacking of large numbers of particles in optical tweezers using a single Gaussian beam. By extending this to multiple trapping sites, formed in the interference pattern generated between two annular (Laguerre-Gaussian) light beams, we have created 3D trapped structures. Furthermore, we use the angular Doppler effect to achieve continuous and controlled rotation of the 3D structure.

The mechanism for creating particle stacks

depends on whether the trapping laser propagates in the direction of gravity (standard tweezers) or against gravity (inverted tweezers). High refractive index silica particles in water tend to sink to the bottom of a sample cell. To create a stack of spheres in standard tweezers, one must therefore optically trap them to allow them to be lifted off the bottom of the sample cell (3D trapping). Once a particle is lifted up by the tweezing laser, the other particles align underneath it, creating a stack.

In an inverted optical tweezers geometry, the laser is focused at the top of the sample cell in such a way that it forms a cone, the widest cross section of which is at the bottom of the sample cell. Dielectric spheres are captured and guided upward within the cone to the focal region of the laser beam, aligning themselves in a vertical stack. The stack height in both geometries is limited by the divergence of the laser beam and the working distance of the microscope objective. Our experimental optical tweezers geometry uses a 200-mW laser, operating at 1064 nm, directed through a ×63 microscope objective (Numerical Aperture 0.95). In the inverted geometry, we have stacked as many as 16 spheres (5 μm in diameter) and have moved the chain as a whole across the sample slide. By tilting the tweezing laser beam, stacks of spheres have been inclined, and angles of 5° have been achieved. Figure 1 shows experimental data for stacking of particles in an inverted optical tweezers geometry. Combining the ability to stack particles with the use of multiple tweezing sites, using either inverted or standard optical tweezers, results in a technique for the creation of a 3D structure.

Single-ringed Laguerre-Gaussian (LG) light beams are described by the index l, which corresponds to the number of 2π cycles of phase around the mode circumference (*14*). Interfering an LG ($l \neq 0$) beam collinearly with a plane wave produces a pattern consisting of l spiral arms that may be used for the rotation of trapped particles (*8*). However, the form of this pattern is determined by the mismatch in both the Gouy phase of each of the two beams and their respective wavefront curvatures, causing the pattern to exhibit marked azimuthal intensity variations as the pattern propagates away from a focus (*15*). We demonstrate an interference pattern that overcomes these limitations and propagates without change of form in space (apart from radial scaling), allowing the stacking of particles in each bright region of the pattern. Specifically, an LG beam of index l is interfered with its mirror image (index $-l$, opposite beam helicity), resulting in a spatial pattern of $2l$ spots arranged on the circumference of a ring (Fig. 2). Related patterns have been analyzed in other studies (*16*–*18*).

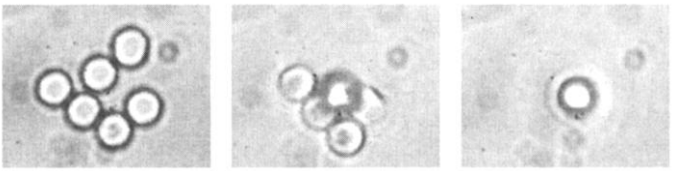

Fig. 1. Assembly of a stack of six trapped particles (each 53 μm in diameter) in inverted tweezers. The stack is fully translatable across the sample slide (1 cm in diameter) at 200 μm/s using a tweezing laser power of 200 mW.

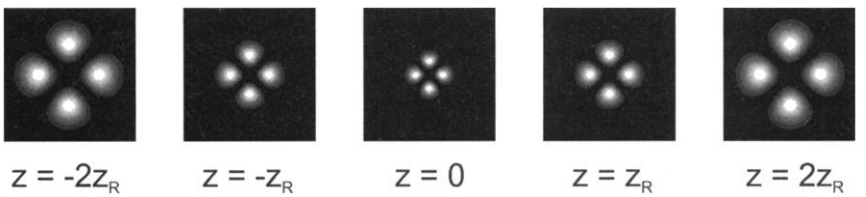

Fig. 2. The interference pattern between two LG beams of opposite helicity but of the same beam parameters ($l = 2$ and an LG beam of $l = -2$). The pattern is shown at the focal point and at various transverse planes up to twice the Rayleigh range (z_R). Each of the constituent LG beams has the same Gouy phase and wavefront curvature, which allows the pattern to propagate without change of form.

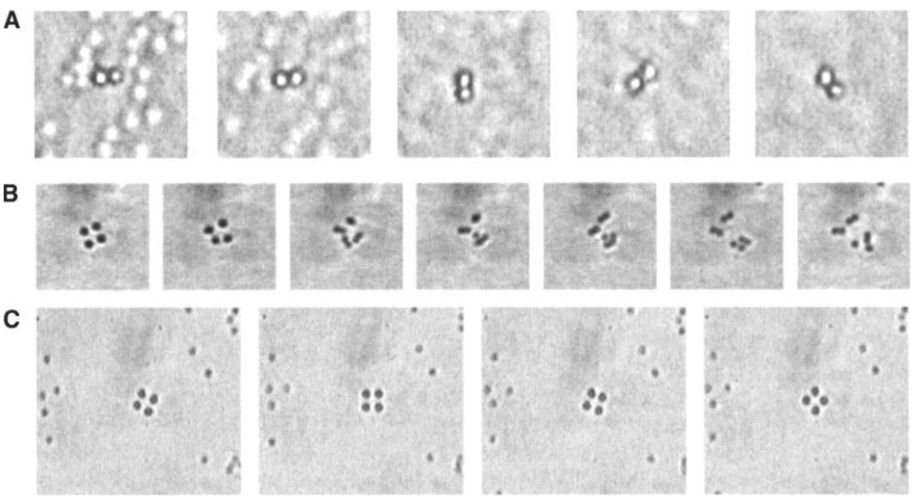

Fig. 3. (A) A group of four 1-μm-diameter spheres, tweezed and lifted vertically (whilst simultaneously rotated) through the sample cell using a LG interference pattern with beams of $l = 1$ and $l = -1$. View from above; only the top two spheres are visible. **(B)** A cubic structure created in optical tweezers with the interference pattern of Fig. 2. The laser beam is blocked and the cubic structure seen in the left-most frame collapses, revealing the eight constituent spheres of the structure (right-most frame). **(C)** The cubic structure of Fig. 3B is trapped in three dimensions. It is rotated using the angular Doppler effect at rates up to 2 Hz.

The experimental setup for tweezing using the interference pattern is similar to that used in previous work (*8*). The LG laser beam is generated from a holographic element and passed through a Mach-Zehnder interferometer. A dove prism is placed in one arm of the interferometer, which creates a mirror image of the beam and inverts the handedness of the helical wavefront of the beam in that arm. The beams are superimposed collinearly at the output to give the interference pattern (Fig. 2). This pattern is then directed into an optical tweezers setup as described previously.

In addition to the lateral and vertical motion of the pattern, we can induce the pattern to rotate around its axis of symmetry using the angular Doppler effect (*19*). A frequency difference is induced between the two arms of the interferometer, resulting in the rotation of the whole interference pattern of spots at a frequency of Ω/l, where Ω is the rotation rate of a half-wave plate in one arm of the interferometer. The rotation of this pattern is a consequence of the helical wavefronts of each of the LG beams. The angular Doppler effect is a very simple and effective way to introduce the relatively small frequency difference required (from less than 1 Hz to 1 kHz)

[1]School of Physics and Astronomy, St. Andrews University, North Haugh, St. Andrews, Fife KY16 9SS, Scotland. [2]Instituto Nacional de Astrofísica, Optica y Electrónica, Apartado, Postal 51/216, 72000 Puebla, Puebla, Mexico 72000. [3]COSMIC, Department of Physics and Astronomy, The University of Edinburgh, The King's Buildings, Edinburgh EH9 3JZ, Scotland.

*To whom correspondence should be addressed. E-mail: kd1@st-and.ac.uk

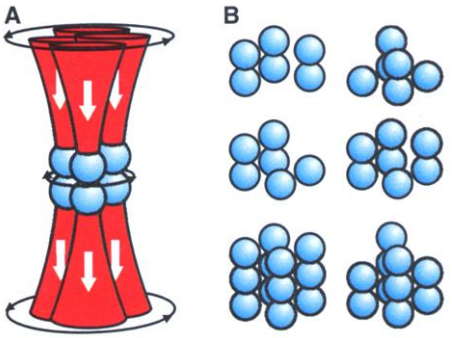

Fig. 4. (**A**) The geometry of the interference pattern that leads to the data of Fig. 3, B and C. (**B**) Diagrams of various other trapped structures, including asymmetric structures, which we have assembled experimentally in our optical tweezers.

between two light beams for the controlled rotation of an interference pattern. This technique can be applied in any situation where slow motion of an interference pattern is desired, such as translating particles in simple linear interferometric tweezers (*20*) or creating a moving "conveyor belt" of dipole traps for deterministic delivery of ensembles of cold atoms (*21*).

The angular Doppler effect makes use of the fact that circularly polarized light reverses its handedness when passing through a half-wave plate. Thus a change in spin angular momentum of $2\hbar$ per photon occurs as the light passes through this optical element. If the wave plate now rotates, energy can be exchanged between the rotating plate and the light beam, causing either an increase or decrease in the frequency of the light beam (*22*). In our system, a rotating half-wave plate is used, but this could be replaced by an electro-optic crystal to mimic this effect and therefore offers a system that would have no moving parts.

Different versions of the interference pattern between two LG beams of opposite helicity have been used for studies of various groups of trapped particles. The pattern is directed, in our tweezers geometry, into a sample cell containing 1-μm silica spheres dispersed in water. Using a pattern formed by superimposing an $l = 1$ beam onto an $l = -1$ beam (two spots), we have tweezed and rotated several rodlike particles including chromosomes. Groups of spheres have been rotated and simultaneously translated vertically through the sample slide, thus giving full 3D control (Fig. 3A). Interfering an $l = 2$ and $l = -2$ LG beam creates a 3D light intensity distribution suitable for the creation of cubic structures (Fig. 3B and Fig. 4A). By adjusting the sample stage, we were able to tweeze particles into the bright regions, forming four separate stacks, each with two spheres, creating a 3D cubic structure (Fig. 3B). In Fig. 3B, the light beam is blocked and the 3D structure (seen complete in the first frame) collapses to reveal the eight constituent 1-μm (in diameter) spheres. The structure is rotated using the angular Doppler effect (Fig. 3C). We also stacked additional particles in each bright region, creating different cubic structures. By controlling the number of spheres loaded in each bright region, we created asymmetric 3D structures (Fig. 4B). Our propagating interference pattern can be combined with a standing wave to offer discrete trapping sites in the axial direction (*23*). The creation and manipulation of artificial structures (such as those in Fig. 4B) at or just below the micrometer level is of current interest in colloid physics. Our ensemble of trapped particles can act as a predetermined nucleus for subsequent growth of novel crystalline structures by self-assembly.

References and Notes

1. A. Ashkin, J. M. Dziedzic, J. E. Bjorkholm, S. Chu, *Opt. Lett.* **11**, 288 (1986).
2. A. Ashkin, J. M. Dziedzic, T. Yamane, *Nature* **330**, 769 (1987).
3. S. B. Smith, Y. Cui, C. Bustamante, *Science* **271**, 795 (1996).
4. M. E. J. Friese, T. A. Nieminen, N. R. Heckenberg, H. Rubinsztein-Dunlop, *Nature* **394**, 348 (1998).
5. E. Higurashi, R. Sawada, T. Ito, *Phys. Rev. E* **59**, 3676 (1999).
6. N. B. Simpson, K. Dholakia, L. Allen, M. J. Padgett, *Opt. Lett.* **22**, 52 (1997).
7. P. Galajda, P. Ormos, *Appl. Phys. Lett.* **78**, 249 (2001).
8. L. Paterson *et al.*, *Science*, **292**, 912 (2001).
9. E. R. Dufresne, G. C. Spalding, M. T. Dearing, S. A. Sheets, D. G. Grier, *Rev. Sci. Instrum.* **72**, 1810 (2001).
10. R. L. Eriksen, P. C. Mogensen, J. Glückstad, *Opt. Lett.* **27**, 267 (2002).
11. P. Zemánek, A. Jónaš, L. Šrámek, M. Liška, *Opt. Lett.* **24**, 1448 (1999).
12. J. Arlt, V. Garcés-Chávez, W. Sibbett, K. Dholakia, *Opt. Commun.* **197**, 239 (2001).
13. R. C. Gauthier, M. Ashman, *Appl. Opt.* **37**, 6421 (1998).
14. L. Allen, M. W. Beijersbergen, R. J. C. Spreeuw, J. P. Woerdman, *Phys. Rev. A* **45**, 8185 (1992).
15. M. P. MacDonald *et al.*, *Opt. Commun.* **201**, 21 (2002).
16. R. Piestun, Y. Y. Schechner, J. Shamir, *J. Opt. Soc. Am. A* **17**, 294 (2000).
17. Y. Y. Schechner, R. Piestun, J. Shamir, *Phys. Rev. E* **54**, R50 (1996).
18. A. A. Tovar, *J. Opt. Soc. Am. A* **17**, 2010 (2000).
19. B. A. Garetz, *J. Opt. Soc. Am.* **71**, 609 (1981).
20. A. E. Chiou, W. Wang, G. J. Sonek, J. Hong, M. W. Berns, *Opt. Commun.* **133**, 7 (1997).
21. S. Kuhr *et al.*, *Science*, **293**, 278 (2001).
22. F. Bretenaker, A. Le Floch., *Phys. Rev. Lett.* **65**, 2316 (1990).
23. M. M. Burns, J. M. Fournier, J. A. Golovchenko, *Science* **249**, 749 (1990).

24. We thank the UK Engineering and Physical Sciences Research Council, The Royal Society Paul Instrument Fund, and the Medical Research Council for supporting this research and W. C. K. Poon for useful discussions. K.V.S. acknowledges the support of CONACYT, Mexico and S. Chávez-Cerda.

7 January 2002; accepted 25 March 2002

Single-Molecule Optomechanical Cycle

Thorsten Hugel,[1] Nolan B. Holland,[1]* Anna Cattani,[2] Luis Moroder,[2] Markus Seitz,[1] Hermann E. Gaub[1]†

Light-powered molecular machines are conjectured to be essential constituents of future nanoscale devices. As a model for such systems, we have synthesized a polymer of bistable photosensitive azobenzenes. Individual polymers were investigated by single-molecule force spectroscopy in combination with optical excitation in total internal reflection. We were able to optically lengthen and contract individual polymers by switching the azo groups between their trans and cis configurations. The polymer was found to contract against an external force acting along the polymer backbone, thus delivering mechanical work. As a proof of principle, the polymer was operated in a periodic mode, demonstrating for the first time optomechanical energy conversion in a single-molecule device.

Nanomechanical devices or molecular machines will, for a broad range of applications, most likely be powered by light or other kinds of electromagnetic radiation (*1–4*). The dominant reasons are ease of addressability, picosecond reaction times to external stimuli, and compatibility with a broad range of ambient substances, such as solvents, electrolytes, gases, or vacuum. One of the key challenges, not only in the development phase but also in operation, is the need to interface such nanometer-sized or molecular devices with the macroscopic world. Single-molecule force spectroscopy by atomic force microscope (AFM) techniques has in the past proven to be an extremely successful strategy (*5–16*). Successful attempts to use an AFM tip to guide the activity of enzymes have paved the road toward a molecular machine tool (*17*).

We now combine single-molecule mechanics with optics to excite an ensemble of molecules and mechanically select an individual molecule from this ensemble. As the photoactive system, we used a polymer of azobenzene units (Fig. 1). This well-studied chromophore, which can be reversibly

[1]Lehrstuhl für Angewandte Physik & Center for Nanoscience, Ludwig-Maximilians Universität, Amalienstrasse 54, 80799 München, Germany. [2]Max-Planck-Institut für Biochemie, Am Klopferspitz 18 a, 82152 Martinsried, Germany.

*Present address: Department of Physiology and Biophysics, Case Western Reserve University, 10900 Euclid Avenue, Cleveland, OH 44106, USA.
†To whom correspondence should be addressed.